

**The effects of relaxation on conversion negative electrode materials for Li-ion batteries:  
a study of TiSnSb using  $^{119}\text{Sn}$  Mössbauer and  $^7\text{Li}$  MAS NMR spectroscopies**

Karen E. Johnston,<sup>1,2□\*</sup> Moulay T. Sougrati,<sup>3,4</sup> Lorenzo Stievano,<sup>3,4</sup> Ali Darwiche,<sup>3,4</sup> Nicolas Dupré,<sup>1</sup> Clare P. Grey<sup>2</sup> and Laure Monconduit<sup>3,4</sup>

<sup>1</sup>Institut des Matériaux Jean Rouxel (IMN), CNRS UMR 6502, Université de Nantes, 44322,  
Nantes Cedex 3, France

<sup>2</sup>Department of Chemistry, University of Cambridge, Lensfield Road, Cambridge, CB2 1EW,  
United Kingdom

<sup>3</sup>Institut Charles Gerhardt Montpellier-UMR 5253 CNRS, ALISTORE European Research  
Institute (3104 CNRS), Université Montpellier 2, 34095, Montpellier, France

<sup>4</sup>Réseau sur le Stockage Electrochimique de l'Energie (RS2E), FR CNRS 3459, France

\*Author to whom correspondence should be addressed

□Current Address: Department of Chemistry, Durham University, Durham, DH1 3LE, United  
Kingdom

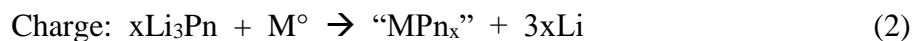
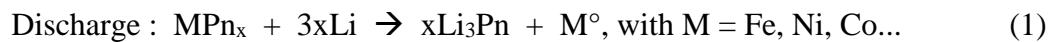
Electronic mail: karen.johnston@durham.ac.uk

## Abstract

Conversion materials were recently considered as plausible alternatives to conventional insertion negative electrode materials in lithium-ion batteries due to their large gravimetric and volumetric energy densities. The ternary alloy TiSnSb was recently proposed as a suitable negative electrode material due to its large capacity ( $550 \text{ mA h g}^{-1}$ ) and rate capability over many cycles. TiSnSb has been investigated at the end of lithiation (discharge) using  $^{119}\text{Sn}$  Mössbauer and  $^7\text{Li}$  magic-angle spinning (MAS) NMR spectroscopies to determine the species formed, their relative stabilities and their behaviour during relaxation. During discharge, TiSnSb undergoes a conversion reaction to produce a mixture of phases believed to consist of lithium antimonides, lithium stannides and titanium metal. *In situ*  $^{119}\text{Sn}$  Mössbauer spectroscopy data indicates the presence of  $\text{Li}_7\text{Sn}_2$  at the end of discharge, while  $^7\text{Li}$  NMR experiments suggest the formation of two distinct Sn-containing species (tentatively assigned to  $\text{Li}_7\text{Sn}_2$  and  $\text{Li}_7\text{Sn}_3$ ), in addition to two Sb-containing species (tentatively assigned as  $\text{Li}_3\text{Sb}$  and a non-stoichiometric phase of  $\text{Li}_2\text{Sb}$ ,  $\text{Li}_{2-x}\text{Sb}$ ). To gain insight into the relative stabilities of the species formed, experiments have been completed under open circuit voltage conditions. A new Sn-based species has been identified via  $^{119}\text{Sn}$  Mössbauer spectroscopy at the end of relaxation. Similar changes are observed in the  $^7\text{Li}$  NMR spectra obtained during relaxation. The species created at the end of discharge are extremely unstable and spontaneously evolve towards delithiated phases. Surprisingly, it is possible to resume electrochemical cycling after relaxation. It is likely that this behaviour can be extended to this family of electrode materials that undergo the conversion reaction.

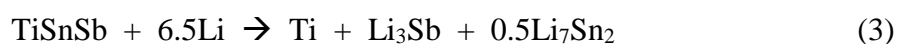
## Introduction

Lithium rechargeable batteries are considered the technology of choice for an array of devices and applications due to their high energy densities.<sup>1,2</sup> There are, however, limitations to the energy densities of electrode materials, most commonly caused by low capacities and limited cycle lives. Conversion type materials have recently been considered as plausible alternatives to conventional insertion electrode materials, due to their large gravimetric and volumetric energy densities.<sup>2-10</sup> Using this class of materials, an uptake of up to nine Li per transition metal is possible in pnictides, when compared to only one or two Li per transition metal in classical insertion materials.<sup>2,3</sup> Upon complete conversion, metallic nanoparticles and binary lithium compounds (*e.g.*, Li<sub>3</sub>Pn in the case of pnictides, Pn = P, Sb) are formed. The key to the reversibility of the conversion reaction is believed to be the well connected nanocomposite structure obtained at the end of discharge. The reaction expected to occur can be summarized as:



Recent studies have shown that the composite obtained at the end of discharge is particularly unstable.<sup>11</sup> However, to date, few studies have addressed the physico-chemical mechanisms causing this instability, or explained the consequences of this behaviour on the relaxation of the associated battery. Any instabilities observed in lithiated electrodes are relevant in all conversion intermetallic phases used as negative electrodes, as well as in alloying systems, such as silicon-based electrode materials.<sup>12,13</sup> The consequences of such features are key for their use in batteries (*e.g.*, self discharge) and must be understood if commercialization is planned.

The ternary alloy TiSnSb has recently been proposed as a suitable negative electrode material in Li-ion batteries due to its excellent electrochemical performance.<sup>14-17</sup> TiSnSb is known to undergo a conversion reaction, leading to reversible capacities of 540 mA h/g or 4070 mA h/cm<sup>3</sup> at a rate of 2C (2 Li per formula unit in 1 hr) and the formation of Li-Sn and Li-Sb intermetallics.<sup>14</sup> The discharge mechanism of TiSnSb was first reported in reference 14, where the corresponding, albeit simplified, electrochemical equation was proposed for Li insertion:



However, the charge mechanism is not yet fully understood due to the amorphous nature of the charged electrode. Different hypotheses have been proposed for the structure of the charged electrode, such as the presence of mixed phases or the formation of a ternary alloy close to TiSnSb.<sup>14</sup>

Previous <sup>7</sup>Li magic-angle spinning (MAS) NMR studies completed for TiSnSb raised questions regarding the phases formed upon discharge and their relative stabilities.<sup>16</sup> We have therefore chosen to investigate the chemical stabilities of the lithiated phases formed at the end of discharge using TiSnSb as a model compound for low potential conversion materials, as many of the processes observed here are believed to be general for other low potential conversion materials. Using <sup>7</sup>Li NMR alone it is difficult to definitively identify all of the species formed and, in such cases, the use of different, complementary techniques is necessary. Furthermore, the comparison of both *in situ* and *ex situ* results can aid in identifying any unknown species. In the present study information obtained from both <sup>119</sup>Sn Mössbauer and <sup>7</sup>Li MAS NMR studies have been used to gain a deeper understanding of the species formed upon lithiation and subsequent relaxation of a TiSnSb electrode. Experiments have been performed during both real time and after a period of relaxation.

The first part of this paper briefly describes the electrochemical performance of TiSnSb. Then, using  $^{119}\text{Sn}$  Mössbauer and  $^7\text{Li}$  MAS NMR spectroscopies, the behaviour of TiSnSb is monitored during discharge. In the second part of the paper, both techniques are used to investigate the evolution of the lithiated phases within an *in situ* cell, *i.e.*, the fate of the phases in a discharged electrode during the relaxation process inside the cells and in the presence of the electrolyte are followed. These results are then compared to those obtained during *ex situ* relaxation of the lithiated electrode material, where we study the discharged electrode after it is rinsed, dried and stored outside the cell.

## Experimental

*Electrode Preparation.* To prepare electrodes, carboxymethyl cellulose (CMC) (degree of substitution DS = 0.7, and average molecular weight  $M_w = 250,000 \text{ g mol}^{-1}$ , Aldrich) was used as a binder with two conductive additives: (i) vapor-grown carbon fibers (VGCF, diameter 100-200 nm and length 10-20  $\mu\text{m}$ , Brunauer-Emmett-Teller (BET) surface area  $15 \text{ m}^2 \text{ g}^{-1}$ , SHOWA DENKO) and (ii) carbon black Y50A (CB, BET primary particle size 20-60 nm, primary aggregate size 100 nm, surface area  $70 \text{ m}^2 \text{ g}^{-1}$ ). The TiSnSb powder, CMC, and additives were manually ground in a mortar and pestle with a weight ratio of 70/12/9/9% (TiSnSb/CMC/Y50A/VGCF). The mixture was mixed with deionised water in a silicon nitride vial containing three 9.5 mm diameter silicon nitride balls and using a Fritsch Pulverisette 7 the mixture was milled at 500 rpm for 1 hour. The slurry was tape cast onto 22  $\mu\text{m}$  thick copper foil at 150  $\mu\text{m}$  thickness. The electrodes were then dried for 12 h at room temperature and for 1 h at 100  $^\circ\text{C}$  under vacuum.

*Electrochemical Tests.* TiSnSb electrodes were cycled against Li metal with  $\text{LiPF}_6$  1 M in EC:PC:3DMC-VC. Each cell was assembled inside an argon-filled glovebox. Electrochemical discharge curves were recorded on a multi-channel VMP system under galvanostatic conditions at rates of C/2 and 4C down to 10 mV vs.  $\text{Li}^+/\text{Li}$ . After reaching this potential, the cells were left to relax under open circuit voltage (OCV) conditions.

*Operando*  $^{119}\text{Sn}$  Mössbauer experiments were performed in a specially designed Swagelok<sup>TM</sup> *in situ* cell equipped with beryllium windows, using a cycling rate of C/2.<sup>18</sup> All *in situ* cells were tested extensively for air- and moisture-tightness and were deemed to be fully airtight. Initial electrochemical tests for  $^7\text{Li}$  MAS NMR experiments were completed using conventional two-electrode Swagelok<sup>TM</sup> cells. To compare with the Mössbauer experiments, all relaxation experiments were carried out using two-electrode Swagelok<sup>TM</sup>-

type cells initially designed for *in situ* X-ray diffraction experiments, with two beryllium windows. In all cases, the cells were disassembled in a glovebox, where the active materials were extracted, rinsed with dimethyl carbonate (DMC), dried and packed into 2.5 mm zirconia rotors for immediate NMR analysis.

*<sup>119</sup>Sn Mössbauer Spectroscopy.* Transmission <sup>119</sup>Sn Mössbauer spectra were recorded in constant acceleration mode. During all experiments both the Ca<sup>119m</sup>SnO<sub>3</sub> source (with an activity of 10 mCi) and the absorber were kept at room temperature. The velocity scale was calibrated using the magnetically split sextet spectrum of high-purity  $\alpha$ -Fe foil as the reference absorber, using a <sup>57</sup>Co (Rh) source. The spectra were fitted to appropriate combinations of Lorentzian profiles by least-squares methods using the program PC-Ms II.<sup>19</sup> Using this method, parameters such as the quadrupole splitting ( $\Delta$ ), the isomer shift ( $\delta$ ), the linewidth ( $\Gamma$ ) and the relative resonance areas of the different spectral components were determined.

*Solid-State NMR Spectroscopy.* All room temperature <sup>7</sup>Li and <sup>19</sup>F MAS NMR spectra were acquired using Bruker Avance 200 and 500 MHz spectrometers, equipped with wide-bore 4.7 T and 11.8 T magnets using Larmor frequencies of 77.9 MHz and 470 MHz for <sup>7</sup>Li ( $I = 3/2$ ) and <sup>19</sup>F ( $I = 1/2$ ), respectively. The powdered samples were packed into conventional 2.5 mm zirconia rotors and an MAS rate of 25 kHz was employed. <sup>7</sup>Li and <sup>19</sup>F chemical shifts were referenced to 1 M LiCl (aq) at  $\delta_{\text{iso}} = 0.0$  ppm and neat CFC<sub>3</sub> (l) ( $\delta_{\text{iso}} = 0.0$  ppm) using Teflon (C<sub>2</sub>F<sub>4</sub>)<sub>n</sub> ( $\delta_{\text{iso}} = -122.0$  ppm) as a secondary reference, respectively. In order to eliminate signal corresponding to the probe, <sup>7</sup>Li and <sup>19</sup>F NMR spectra were acquired using a Hahn echo (90 –  $\tau$  – 180 –  $\tau$ ) pulse sequence. Optimized recycle intervals for <sup>7</sup>Li and <sup>19</sup>F were 30 and 15 s, respectively. Spectral analysis and fitting were performed within the Dmfit software package.<sup>20</sup> All samples, unless where stated in the text, were washed three times with DMC immediately after disassembling the cells and prior to analysis.

Two-dimensional magnetization exchange  $^7\text{Li}$  NMR spectra were acquired using the sequence  $(\pi/2)-\tau_1-(\pi/2)-\tau_m-(\pi/2)-\tau_2\text{-acq}$ , where  $\tau_1$  and  $\tau_2$  represent interpulse delays and  $\tau_m$  represents the mixing time. A range of mixing times were tested, including 1, 20, 100 and 200 ms.

## Results and Discussion

### *Electrochemistry*

During this study three different electrochemical cells have been used to study TiSnSb. A specially designed *in situ* Swagelok™ cell equipped with two beryllium windows has been used for the *in situ*  $^{119}\text{Sn}$  Mössbauer study. For NMR experiments, conventional Swagelok™ cells and two-electrode Swagelok™-type cells with two beryllium windows have been used. Typical discharge/relaxation curves obtained for TiSnSb/Li using the *in situ* Mössbauer cell (blue) and the two-electrode Swagelok™-type cell with beryllium windows (red) are shown in Figure 1. In both cases, during discharge down to 10 mV a rapid decrease in potential from an open circuit voltage (OCV) of 1.2 V to 0.8 V is observed, assigned to formation of the solid-electrolyte interphase (SEI). This is followed by a redox process around 0.25 V. As in all conversion type materials, TiSnSb undergoes a specific low voltage discharge. The voltage profile exhibits a progressive decrease and is characteristic of the ternary alloy TiSnSb.<sup>14</sup> No distinct or separate processes are observed for the lithiation of tin and antimony. At the end of discharge approximately 7 Li per formula unit (theoretically, the reaction of 6.5 Li according to the formation of  $\text{Li}_3\text{Sb}$  and  $\text{Li}_7\text{Sn}_2$ ) are inserted into the TiSnSb structure, in good agreement with previous findings.<sup>14,15</sup> In each case, after reaching a cut-off potential of 10 mV, both cells were allowed to undergo ‘relaxation’ under OCV conditions. Immediately after discharge, a rapid increase in potential is observed for both experiments. Once a potential of 80 mV is attained, the potential slowly increases. During the *in situ*  $^{119}\text{Sn}$  Mössbauer experiment, a gradual increase in potential is observed during OCV relaxation, reaching ~0.54 V in 150 hours (blue curve in Figure 1). This is in contrast to the corresponding NMR experiment, where the increase in potential is considerably faster, as demonstrated by the red curve in Figure 1. It is noted that the behaviour exhibited in each cell

is fully reproducible. To successfully combine the Mössbauer and NMR data, comparisons will be made between samples with the same state of charge (*i.e.*, similar OCV potentials).

### *Behaviour During and At the End of Discharge*

#### *In Situ $^{119}\text{Sn}$ Mössbauer Spectroscopy*

The *in situ*  $^{119}\text{Sn}$  Mössbauer spectra collected during discharge of  $\text{TiSnSb}$  are shown in Figure 2. As observed in a previous study, the *operando* spectra start to exhibit significant changes after the reaction of approximately 1 Li per formula unit.<sup>14</sup> This confirms that the initial electrochemical activity is due to the reaction of Li with the electrolyte and/or other surface phenomena (*i.e.*, formation of the SEI). After this period, the initial quadrupole doublet typical of  $\text{TiSnSb}$  is slowly transformed into new spectral components with hyperfine parameters in the range expected for Li-Sn intermetallics.<sup>16</sup> Comparing the mean isomer shift values, which are known to decrease with increasing lithium content, it is possible to follow the formation of Li-Sn intermetallics with changing lithium/tin ratios. At the end of discharge, after approximately 14 hours of reaction (Figure 2(d)), the isomer shift reaches almost  $1.9 \text{ mm s}^{-1}$ , close to the value typically observed for  $\text{Li}_7\text{Sn}_2$ .<sup>21</sup> However, the spectrum obtained does not reproduce the spectral signature of pure  $\text{Li}_7\text{Sn}_2$  previously reported by Robert *et al.* and Dunlap *et al.*<sup>21,22</sup> This result is in line with previous observations for Sn-based negative electrode materials and suggests that an ill-defined and/or nanostructured form of  $\text{Li}_7\text{Sn}_2$  is formed at the end of lithiation of  $\text{TiSnSb}$ .<sup>23</sup> Alternatively, additional tin-based lithiated species with similar Li content could also be present. For example,  $\text{Li}_7\text{Sn}_3$  ( $\langle\delta\rangle = 2.02 \text{ mm s}^{-1}$ ).<sup>21,22</sup>

## <sup>7</sup>Li MAS NMR

To determine the phases formed at the end of discharge, three samples of TiSnSb were initially prepared for NMR analysis using a standard Swagelok™ cell. The first two samples were discharged to a cut-off potential of 10 mV at rates of C/2 and 4C, denoted by points (1) and (2), respectively on the discharge profiles shown in Figure 3(a). To determine whether the cycling rate affects the phases formed, two different rates were tested (one fast and one slow). The third sample (3) was discharged at a rate of C/2 and stopped when a capacity equal to that of the second sample was attained, this corresponds to a cut-off potential of 18 mV. Immediately after discharge each cell was disassembled and no relaxation step was allowed. The <sup>7</sup>Li MAS NMR spectra obtained for the three samples are shown in Figure 3(a). In all cases, two distinct groups of resonances are observed, one centred at 3.5 ppm and the second characterized by a significant shift at 20 ppm. The resonances are broad and partially overlapped, which prevents an unambiguous deconvolution of each spectrum.

The spectrum obtained for sample (1) was simulated and is shown in Figure 3(b). To simulate the two groups of resonances observed, multiple lineshapes were required. Attempts were made to simulate the spectrum using two resonances, centred at 3.5 and 20 ppm. However, this was not sufficient to accurately simulate the lineshape and it was concluded that the second group of resonances must be deconvoluted into two resonances at 19.5 and 22 ppm, respectively. <sup>7</sup>Li NMR spectra obtained at the end of the first discharge contain resonances corresponding to lithium nuclei both within alloys and in the SEI. To estimate the SEI contribution, to a first approximation, we considered the <sup>7</sup>Li signal obtained after one full cycle, *i.e.*, at the end of a complete delithiation (end of charge), as this, in principle, corresponds only to the lithium nuclei trapped irreversibly in the SEI. The <sup>7</sup>Li NMR spectrum obtained at the end of the first charge was simulated (Figure S1) and the contribution from the SEI was identified at 2.3 ppm and corresponds to approximately 20% of the total integrated

intensity. Considering the voltage vs. composition curves of TiSnSb, a large irreversible capacity is observed in the first cycle, *i.e.*, 6.5 Li are inserted during lithiation, in addition to SEI formation, and at the end of oxidation there are 1.2 Li or electrons that remain trapped irreversibly. The lithiation of TiSnSb appears to be completely reversible as there are no traces of Li<sub>3</sub>Sb or Li<sub>7</sub>Sn<sub>2</sub>. Hence, the large irreversible capacity observed appears to correspond to SEI formation and it is 18% of the total capacity. Hence, it is correct having an SEI contribution of around 20%. It is noted that the SEI shift is larger than typically observed for the SEI,<sup>24,25</sup> suggesting a component could be Li<sub>2</sub>O. The contribution at 3.5 ppm is most likely attributed to Li<sub>3</sub>Sb. This is based on our recent study on the lithiation of Sb, where the depth of lithiation was studied extensively, as detailed in reference 27. The smaller contribution at 8.5 ppm is tentatively assigned to Li<sub>7</sub>Sn<sub>2</sub>. This assignment is based on the <sup>119</sup>Sn Mössbauer data (*vide supra*), the chemical shift of 9 ppm reported in the literature<sup>26</sup> and our recent studies of Sn-based phases, as detailed in Figure S2 in the Supporting Information. Previous NMR studies have attributed signal at 18 ppm to the intermetallic Li<sub>7</sub>Sn<sub>3</sub>.<sup>26</sup> Based on this, and our own studies of Sn (Figure S2), Li<sub>7</sub>Sn<sub>3</sub> is believed to be present, in addition to Li<sub>7</sub>Sn<sub>2</sub>. It is noted that this phase has never been directly detected via <sup>119</sup>Sn Mössbauer spectroscopy in this or any previous studies. The contributions from Li<sub>3</sub>Sb, Li<sub>7</sub>Sn<sub>2</sub> and Li<sub>7</sub>Sn<sub>3</sub>, based on deconvolution of the <sup>7</sup>Li MAS NMR spectrum in Figure 3(b), account for approximately 24%, 11% and 34% of the total integrated intensity, respectively. The intensity of the resonance corresponding to Li<sub>3</sub>Sb is too small to match the contribution of the Sn-based phases formed (see equation (3)). It is known from previous <sup>121</sup>Sb Mössbauer studies that no unreacted or pure Sb is present at the end of discharge.<sup>15</sup> Hence, in order to balance the electrochemical equation and account for the missing Sb there must be an additional Li-Sb alloy present. While we recognise there are some errors associated with the contribution of the SEI, it is likely that the group of resonances at 20 ppm includes a

contribution from a Li-Sb alloy, in addition to the Li-Sn alloy tentatively assigned to  $\text{Li}_7\text{Sn}_3$ . Based on this deconvolution, we have assigned the peak at 22 ppm to a second Li-Sb alloy. We know from two-dimensional  $^7\text{Li}$  NMR exchange experiments that the lithium environments giving rise to the resonances at 20 and 3.5 ppm belong to distinct species (see Figure S3 in the Supporting Information for further details). Hence, if the resonance at 3.5 ppm is correctly assigned to  $\text{Li}_3\text{Sb}$ , the other resonance must be a different species that cannot be detected by XRD.<sup>14,15</sup>

The lithiation of pure Sb was recently investigated by our research group and, using conventional  $^7\text{Li}$  MAS NMR and two-dimensional  $^7\text{Li}$  exchange experiments, the phases  $\text{Li}_2\text{Sb}$  and  $\text{Li}_3\text{Sb}$  were identified at 40 and  $-17$  ppm, and 3.8 ppm, respectively.<sup>27</sup> During two-dimensional  $^7\text{Li}$  exchange experiments a resonance at 21 ppm was also observed that correlates with the resonances at 40 and  $-17$  ppm, suggesting it is related to the phase  $\text{Li}_2\text{Sb}$ . The resonance was attributed to low concentrations of Li vacancies or interstitials generated during lithiation and the phase was assigned to a non-stoichiometric phase of  $\text{Li}_2\text{Sb}$ , denoted as  $\text{Li}_{2-x}\text{Sb}$ . Based on these findings, the resonance at 22 ppm is tentatively assigned to this phase. The study by Chang *et al.*, which combines both experimental and theoretical data, suggests the structures of both  $\text{Li}_3\text{Sb}$  and  $\text{Li}_2\text{Sb}$  can tolerate some degree of off stoichiometry, caused by the introduction of vacancies during lithiation.<sup>27</sup>

The spectra obtained for samples (2) and (3) are essentially identical. This indicates that, independent of whether samples are cycled at  $C/2$  or  $4C$ , if they are stopped at the same composition, identical NMR spectra will be observed, at least at this state of charge. In contrast, the spectra obtained for samples (1) and (3), which were cycled at the same rate ( $C/2$ ) and stopped at different compositions, exhibit distinct differences in both the relative intensities and chemical shifts of the two resonances. These differences reflect changes in the lithium composition, which may give rise to differences in the number or amount of lithiated

alloys present in the sample. This suggests that alloys giving rise to resonances between 0 and 10 ppm are formed at lower potentials, with respect to the alloys giving rise to resonances at approximately 20 ppm.

### *Behaviour During Relaxation*

#### *In situ $^{119}\text{Sn}$ Mössbauer Spectroscopy*

After reaching the end of discharge, *i.e.*, after 15 hours, the *in situ* cell was allowed to relax under OCV conditions for approximately 150 hours, denoted by the blue curve in Figure 1. During this time  $^{119}\text{Sn}$  Mössbauer spectra were collected each hour and are shown in Figure 4. During the first 36 hours of relaxation (total reaction time of 50 hours, including the 14 hours of discharge) the potential increases from 0 to  $\sim 0.3$  V. During this time there are no visible changes in the Mössbauer spectra. Slight differences occur when potentials greater than 0.3 V are reached, more than 50 hours after the beginning of the discharge.

The spectra were simulated using a single quadrupole doublet. The isomer shift and the quadrupole splitting parameters obtained, together with the spectral full linewidth at half maximum, are shown in Figure 5. These values are not characteristic of a single tin species but, rather, provide a series of average parameters that could correspond to several different species. Both the isomer shift and quadrupole splitting parameters remain constant and within the experimental error of the values measured at the end of discharge. Moreover, no noticeable changes are observed for the linewidth, indicating that, during this period, the lithiated phases are relatively stable and remain unchanged. An increase in the linewidth parameter would indicate inhomogeneity in the sample, possibly caused by partial transformation of the species formed at the end of discharge into a new tin species.

From approximately 35 hours of relaxation (corresponding to a total experimental time of 50 h) an increase in the isomer shift is observed, corresponding to a decrease in the lithiation of the tin species (Figures 4(c) and 5). This is in line with the observed increase in potential.<sup>21</sup> Increases in the quadrupole splitting and linewidth parameters are also evident, indicating a change in the local environment around the tin atoms and, most likely, the presence of inhomogeneities in the composition of the sample. This increase becomes more evident with advancing relaxation, as an increase in potential is accompanied by an increase in both the average quadrupole splitting and isomer shift parameters. After approximately 135 hours of relaxation (total experimental time of 150 hrs) the potential reaches almost 0.6 V, while the isomer shift reaches an average value of 2.1 mm s<sup>-1</sup>. This value is higher than that for Li-rich Li-Sn alloys and approaches that of the starting material TiSnSb (2.19 mm s<sup>-1</sup>). The quadrupole splitting parameter also increases, reaching a value of 1.22 mm s<sup>-1</sup> at the end of relaxation. This is larger than any quadrupole splitting value observed for crystalline Li-Sn intermetallics,<sup>21</sup> but smaller than the value usually observed for TiSnSb (1.70 mm s<sup>-1</sup>).

### *<sup>7</sup>Li MAS NMR*

To monitor the relaxation behaviour of TiSnSb via NMR, experiments were completed in two-electrode Swagelok<sup>TM</sup>-type cells with two beryllium windows. The corresponding voltage-time profile is shown in Figure 1 (red curve). <sup>7</sup>Li MAS NMR spectra (Figure 6) were acquired for TiSnSb electrodes discharged at C/2 and allowed to relax until the potentials shown in Figure 4 were reached. When each potential was attained each cell was stopped and immediately disassembled to prevent any reaction with the remaining electrolyte. The <sup>7</sup>Li MAS NMR spectra shown in Figures 6(a)-(g) correspond to the potentials 0.13, 0.17, 0.22, 0.29, 0.35, 0.44 and 0.55 V, respectively. The spectra acquired for 0.13 V – 0.35 V (Figures 6(a)-(e)) each display two resonances of varying intensity that are centred at approximately 3

and 24 ppm. The spectra corresponding to 0.13 and 0.17 V are very similar to the spectrum obtained at the end of discharge (Figure 3(b)), suggesting that a composition similar to this is observed at these potentials. The relative intensities of the two peaks change with increasing potential (0.22 – 0.35 V) until only a single resonance is observed at 0.44 and 0.55 V (Figures 6(f) and (g)). This changing intensity suggests differences in the compositions of the phases formed and is likely caused by subtle changes in the local Li environments and/or structural rearrangements of unstable lithiated phases (both Li-Sn and Li-Sb alloys). There are distinct differences in the species present at low (0.13 V) and high (0.55 V) potentials. This is believed to be caused by differences in the stabilities of the lithiated phases formed.

Comparing the spectra shown in Figures 3(a) and 6 highlights an interesting trend. The resonance at ~3 ppm in Figure 3(a) is higher in intensity for the sample cycled at C/2 (green). Interestingly, the intensity of this same peak, observed in spectra corresponding to potentials 0.22 – 0.55 V during the relaxation experiments (Figure 6), also increases. This is unusual because an increase in the intensity of this peak is believed to be caused by the insertion of Li, as evidenced by the spectra shown in Figure 3(a), and SEI swelling. However, no additional Li was inserted during the relaxation experiment, as each cell was under OCV conditions. This behaviour could be further indication that unstable lithiated phases are formed at the end of discharge and phase transitions/de-mixing occurs during relaxation. It is also noted that there is an associated increase in potential, which implies there is a loss of Li. If this is the case it suggests that when Li is removed the process by which it occurs is different to that of Li insertion, *i.e.*, the insertion and removal of Li go through different phases. This is further indication that the species at ~20 ppm corresponds to unstable or ‘intermediate’ lithiated phases only formed during the lithiation process. Hence, it is likely the resonance at 22 ppm is correctly assigned to a non-stoichiometric phase of  $\text{Li}_2\text{Sb}$  ( $\text{Li}_{2-x}\text{Sb}$ ).

## *Ex situ Relaxation Studies*

### *<sup>119</sup>Sn Mössbauer Spectroscopy*

<sup>119</sup>Sn Mössbauer spectra were also acquired for a discharged electrode of TiSnSb extracted from the cell (not shown). In a similar manner to the *operando* spectra, gradual changes were observed, namely a progressive shift of the spectra to high velocities and an increase in the splitting of the spectra. In contrast to the spectra acquired under *in situ* conditions, the evolution is faster for the extracted electrode, and changes in the spectra become significant after only a few hours. The evolution of the average Mössbauer parameters, obtained by simulating each spectrum with a single large quadrupole doublet, are shown in Figure 7. During the first few hours the isomer shift increases rapidly, in line with spontaneous delithiation of the discharged electrode. An increase in the quadrupole splitting and linewidth are also observed, believed to correspond to the formation of new delithiated phases.

The final spectrum in this series, obtained after approximately 160 hours, exhibits an asymmetric shape that suggests the presence of at least two different tin species. Analytical simulation of the spectrum, using two spectral components (Figure 8), indicates a dominant component ( $\delta = 2.18 \text{ mm s}^{-1}$ ;  $\Delta = 1.67 \text{ mm s}^{-1}$ ;  $\Gamma = 0.93 \text{ mm s}^{-1}$ ) that accounts for approximately 70% of the total resonance area and has virtually the same parameters as the starting compound TiSnSb.<sup>8</sup> The remainder of the spectrum was simulated using a second component ( $\delta = 2.18 \text{ mm s}^{-1}$ ;  $\Delta = 0.65 \text{ mm s}^{-1}$ ;  $\Gamma = 0.93 \text{ mm s}^{-1}$ ) that could correspond to lithiated tin species, as the parameters fall in a range between those of Li-rich and Li-poor alloys (signals centred around 2 and 2.3  $\text{mm s}^{-1}$ , respectively).<sup>16</sup> The Mössbauer data therefore indicates that relaxation increases the rate of lithium de-mixing from the alloys, and

a compound very similar to the initial TiSnSb is reformed. This appears to be in good qualitative agreement with the  $^7\text{Li}$  NMR data, which observes the disappearance of the resonance at 20 ppm, and an increase in the intensity of the resonance at lower chemical shift.

### *The Response of Lithiated TiSnSb after Relaxation*

The electrochemical cycling of a TiSnSb electrode after relaxation is shown in Figure 9. Independent of whether cycling is resumed in oxidation or reduction, the relaxation time at the end of discharge does not impact the future cycling of TiSnSb electrodes. Since the capacity is determined by the OCV, it does not matter whether it is reached by cycling or by relaxation of the cell. In fact, a period of relaxation appears to benefit the total capacity retention of TiSnSb. This indicates that evolution of the electrode during OCV, as characterized by NMR and Mössbauer spectroscopies, is reversible. After the OCV period, it is possible to re-insert Li into the electrode, as demonstrated in the inset of Figure 9(a). This confirms that a spontaneous delithiation takes place during the relaxation that has no significant influence on the future charging and cycling of the electrode. Similar findings were observed during corresponding NMR experiments, as detailed in Figures S3 and S4. The results indicate that, at the end of relaxation, the lithiated species are transformed back into a compound that closely resembles the initial TiSnSb. This last point is particularly important because recovery of the initial structure can only be explained by assuming an intimate mixture of Ti with the lithiated Sn and Sb species, and optimized interfaces between these nanodomains.<sup>15</sup> This intimate mixture and the substantial reactivity of Ti are probably the driving force behind the recovery of the initial structure, as previously suggested.<sup>15</sup>

### *Evolution Studies*

#### *$^7\text{Li}$ MAS NMR*

Additional  $^7\text{Li}$  NMR experiments were completed to determine the stability of the phases formed at the end of discharge of  $\text{TiSnSb}$ . Using a conventional Swagelok<sup>TM</sup> cell, a sample of  $\text{TiSnSb}$  was discharged to a cut-off potential of 10 mV at a rate of 4C. The cell was immediately disassembled and no relaxation step was allowed. The corresponding  $^7\text{Li}$  NMR spectra are shown in Figure 10. Each spectrum corresponds to 30 minutes of acquisition time and were acquired immediately (red), 6 hours (blue), 24 hours (green) and 3 days (orange) after disassembling the cell. Two distinct resonances are observed at 3 and 20 ppm after reaching the end of discharge. The spectra then exhibit an obvious evolution with time, indicating that some of the alloys formed at the end of the lithiation process are not stable. A clear shift towards lower chemical shift is observed for the resonances around 20 ppm and, after three days, these resonances have disappeared completely, leaving an intense, broad resonance at 3 ppm. As this resonance spans from  $-20$  to 20 ppm, it is reasonable to consider non negligible contributions from SEI (2 ppm) and  $\text{Li}_7\text{Sn}_2$  (9 ppm). The normalized integrated intensity remains constant during the evolution process, indicating no loss of lithium. This evolution is very similar to that observed during the relaxation study, however, here it is considerably faster.

To investigate this behaviour further, two additional experiments were performed. Samples of  $\text{TiSnSb}$  were discharged in conventional Swagelok<sup>TM</sup> cells to a cut-off potential of 20 mV (at rates of C/2 and 4C) and allowed to relax inside the cell for three days. During this time the electrodes remained in constant contact with the electrolyte. The corresponding discharge curves are shown as an inset in Figure 10(b). The  $^7\text{Li}$  NMR spectra obtained at the end of the relaxation process (Figure 10(b)) display two groups of resonances and are very similar to the spectra obtained immediately after discharge and without relaxation (Figure 3). This suggests the electrolyte slows down the evolution process previously identified when the sample was left to age outside of the cell for three days (Figure 10(a)). Hence, the electrolyte

appears to play a key role in the aging process. It is noted that different relaxation behaviour is observed for conventional Swagelok™ cells versus the *in situ* cells used in Figure 1. We tentatively assign these differences to the respective cell designs. The presence of a spring inside the conventional Swagelok™ cell leads to an increase in the contact pressure between the electrodes and the separator. Due to the specific design of the Mössbauer *in situ* cell, such a spring is not possible. Moreover, the inside volume (and actual quantity of the electrolyte) of the *in situ cell* is larger. We believe the faster self-discharge is observed in the case of the *in situ cell* because the internal pressure is lower when compared to the conventional cell. Still, the fast self-discharge observed in the case of the *in situ cell* is not as fast as the self-discharge observed for the rinsed electrodes. It is also noted that in Figure 1, although the electrolyte is present, it cannot stop the evolution or self-discharge process occurring.

The sample cycled at 4C (shown in Figure 10(b)) was stored in a glovebox for an additional three days. The  $^7\text{Li}$  NMR spectra obtained before and after this period of evolution are shown in Figure 10(c) in blue and green, respectively. An evolution process similar to that observed for electrodes recovered immediately after discharge is observed. The narrow signal at 22 ppm (believed to correspond to a non-stoichiometric phase of  $\text{Li}_2\text{Sb}$ ,  $\text{Li}_{2-x}\text{Sb}$ ) exhibits a simultaneous decrease in intensity and a shift to lower chemical shift. The broader signal at 20 ppm also shifts towards lower chemical shift. However, its intensity is less affected. During this evolution, the second group of resonances (2.8 ppm) increases in intensity while shifting towards higher chemical shift (3.3 ppm). This suggests a greater contribution of Li nuclei in the alloys, in particular  $\text{Li}_3\text{Sb}$ . This behaviour is consistent with the assignment of the narrow signal at 22 ppm to  $\text{Li}_{2-x}\text{Sb}$  and suggests that the evolution corresponds to either a change in the composition of the alloys present at the end of discharge or to phase transitions/de-mixing between two Li-Sb phases. This is further confirmation that

the phase  $\text{Li}_{2-x}\text{Sb}$  is an unstable or intermediate phase. Additional evolution studies are presented in Figure S6 in the Supporting Information.

### *<sup>19</sup>F MAS NMR*

<sup>19</sup>F NMR spectra were acquired for TiSnSb electrodes before and after the aging process described above. The <sup>19</sup>F NMR spectra, shown in Figure S7 in the Supporting Information, exhibit characteristic signals at  $-205$  ppm and  $-72$  ppm, which correspond to LiF and dried  $\text{LiPF}_6$  trapped in the SEI, respectively. Similar relative intensities and normalized integrated intensities are observed before and after aging, indicating the SEI does not evolve during aging. See the Supporting Information for further details. It is worth noting that the SEI also contains lithiated carbonate species such as  $\text{ROCO}_2\text{Li}$  and  $\text{Li}_2\text{CO}_3$ , which can play a role in the observed self-discharge process.

### *Explanation of Relaxation Behaviour*

The data presented suggests two distinct processes are occurring during relaxation of TiSnSb. The first is thermodynamic equilibration of the system, where the highly reactive/metastable Li-Sb and Li-Sn phases formed at the end of discharge undergo structural rearrangements and/or phase transitions to produce more intrinsically stable intermetallics. We have previously shown that TiSnSb reacts with Li to simultaneously form  $\text{Li}_3\text{Sb}$ ,  $\text{Li}_x\text{Sn}$  and Ti through a conversion mechanism. This leads to very intimate mixing of the phases. Nanosized interfaces exist between the different phases, resulting in very close contacts. It is this combination of highly reactive species with close contacts (nanosized interfaces) that is responsible for the reversibility of the conversion reaction occurring and the resulting

electrochemical performance. During thermodynamic equilibration subtle modifications in the electrode/electrolyte interfaces also occur. For example, different relaxation rates were observed for electrodes left to age inside versus outside of the cell, indicating the presence of the electrolyte is key. The second process occurring is a spontaneous loss of Li, as evidenced by the NMR, Mössbauer and electrochemical data presented. Possible explanations for this include Li being trapped in the SEI or reaction of the electrode with the electrolyte. However, as demonstrated above, this does not appear to hinder the future cycling of TiSnSb electrodes.

There are three possible explanations for the relaxation behaviour observed: (1) the metastable phases formed at the end of discharge are highly reactive (induced by optimal nanosized interfaces) and therefore react to form different intermetallic phases and ultimately lose lithium, (2) air or moisture entering the cell or (3) reactions at the electrode/electrolyte interface. Since all of the cells were prepared and handled in a glovebox (under an argon atmosphere) it is unlikely that air and moisture entered the cell. Moreover, no oxides or hydroxides are observed in the  $^{19}\text{F}$  or  $^7\text{Li}$  NMR spectra. Hence, it is unlikely that air and moisture are causing the relaxation. The electrolyte, however, was found to play a key role in the relaxation. The  $^{19}\text{F}$  NMR data exhibits similar intensities for LiF ( $-204$  ppm) and dried  $\text{LiPF}_6$  ( $-72$  ppm) before and after aging, indicating that fluorinated species in the SEI are not being consumed during relaxation. We also know from  $^1\text{H}$  NMR studies (not shown) that no protons are generated during the reaction. This suggests that electrolyte decomposition, electrolyte/electrode interactions and a self discharge process are occurring. Hence, the reactive nanocomposite structures formed at the end of discharge, together with their high surface areas, are likely responsible for the relaxation behaviour observed. The intimate mixing and close contact of the highly reactive phases, as well as their subsequent interaction with the electrolyte, are all contributing factors to the relaxation.

## Conclusions

The material TiSnSb has been investigated using  $^7\text{Li}$  NMR and  $^{119}\text{Sn}$  Mössbauer spectroscopies to determine the changes occurring in electrodes during discharge and subsequent relaxation. The results indicate that the species formed at the end of lithiation are unstable and evolve during relaxation. At the end of discharge, lithiated tin species have been identified via  $^{119}\text{Sn}$  Mössbauer spectroscopy that have an average composition close to  $\text{Li}_7\text{Sn}_2$ . Deconvolution of the  $^7\text{Li}$  MAS NMR spectrum obtained revealed the presence of at least four distinct species with peaks at 2.3, 3.5 and 8.5 ppm, corresponding to the SEI,  $\text{Li}_3\text{Sb}$  and  $\text{Li}_7\text{Sn}_2$ , respectively. A second group of resonances at  $\sim 19.5$  ppm and 22 ppm are believed to be  $\text{Li}_7\text{Sn}_3$  and a non-stoichiometric phase of  $\text{Li}_2\text{Sb}$ ,  $\text{Li}_{2-x}\text{Sb}$ .

During *in situ*  $^{119}\text{Sn}$  Mössbauer experiments (in OCV mode), gradual delithiation of the Sn-based species produced a spectral signature indicative of lithium deficient Li-Sn alloys. These results are in good agreement with those of OCV  $^7\text{Li}$  NMR experiments, where the lithiated species at higher chemical shifts (24 ppm) were found to be less stable and progressively disappeared. The more lithiated species (3 ppm) are more stable and resisted evolution.

$^7\text{Li}$  NMR experiments completed for TiSnSb electrodes at the end of discharge revealed an intrinsic instability of the phases formed. The  $^7\text{Li}$  NMR spectra corresponding to samples immediately rinsed and analyzed after discharge exhibited a rapid evolution (over a period of a few hours to three days) from two resonances at  $\sim 20$  and 3 ppm to a single resonance at 3 ppm. The  $^7\text{Li}$  NMR spectra of samples allowed to relax inside the cell for several days prior to analysis exhibited a similar evolution, however, it was considerably slower, occurring over many days. The presence or absence of the electrolyte was found to play a key role in the evolution process, *i.e.*, reactions at the electrode/electrolyte interface.

Similar behaviour was observed during *ex situ*  $^{119}\text{Sn}$  Mössbauer experiments, where a phase close to the initial TiSnSb was reformed upon delithiation of the discharged electrode.

These results are interesting for several reasons. Firstly, and most importantly, this demonstrates that the intimate nanoscale mixing of Ti with the lithiated Sn and Sb species obtained through the conversion reaction is highly reactive. In general it is known that the extreme reactivity of the transition metal particles, as well as the optimized interfaces between the nanosized species in the discharged electrode, are the driving force for reformation of the conversion compounds during charge.<sup>15</sup> In the case of TiSnSb, the metastability is demonstrated by the evolution of the species obtained at the end of discharge and during relaxation. This unstable state was found to be reversible and does not impact the future cycling of TiSnSb. The presence or absence of the electrolyte plays a key role in the evolution of the species obtained at the end of discharge. However, further investigation is required to clarify this point and determine the role of the SEI on the stabilization of the electrode. This point has an important implication for the use of this family of materials in commercial batteries. More specifically, an appropriate matching of conversion materials, formulation, electrolytes and the working potential window could enable stabilization of the discharged electrode and thus allow the application of such materials in commercial batteries.

## Acknowledgments

This research was performed in the framework of the ALISTORE European Research Institute and their Mössbauer and NMR platforms. The authors thank ALISTORE-ERI for its financial support through the postdoc grant of KEJ, the ANR for financial support in the program ICARES (no. ANR-11BS09-009-01). LM thanks all the partners of ICARES project for fruitful scientific discussions.

Supporting Information Available: Additional  $^7\text{Li}$  and  $^{19}\text{F}$  NMR data. This material is available free of charge via the Internet at <http://pubs.acs.org>.

## References

1. Bruce, P. G.; Scrosati, B.; Tarascon, J.-M. Nanomaterials for Rechargeable Lithium Batteries. *Angew. Chem., Int. Ed.* **2008**, 47, 2930-2946.
2. Palacin, M. R. Recent advances in rechargeable battery materials: a chemist's perspective. *Chem. Soc. Rev.* **2009**, 38, 2565-2575.
3. Cabana, J.; Monconduit, L.; Larcher, D.; Palacin, M. R. Beyond Intercalation-Based Li-Ion Batteries: The State of the Art and Challenges of Electrode Materials Reacting Through Conversion Reactions. *Adv. Mater.* **2010**, 22, E170-E192.

4. Poizot, P.; Laruelle, S.; Grugeon, S.; Dupont, L.; Tarascon, J.-M. Nano-sized transition-metal oxides as negative-electrode materials for lithium-ion batteries. *Nature* **2000**, 407, 496-499.
5. Débart, A.; Dupont, L.; Poizot, P.; Leriche, J.-B.; Tarascon, J.-M. A Transmission Electron Microscopy Study of the Reactivity Mechanism of Tailor-Made CuO Particles toward Lithium. *J. Electrochem. Soc.* **2001**, 148, A1266-A1274.
6. Hall, J. W.; Membreno, N.; Wu, J.; Celio, H.; Jones, R. A.; Stevenson, K. J. Low-Temperature Synthesis of Amorphous FeP<sub>2</sub> and Its Use as Anodes for Li Ion Batteries. *J. Am. Chem. Soc.* **2012**, 134, 5532-5535.
7. Gillot, F.; Boyanov, S.; Dupont, L.; Doublet, M.-L.; Morcrette, M.; Monconduit, L.; Tarascon, J.-M. Electrochemical Reactivity and Design of NiP<sub>2</sub> Negative Electrodes for Secondary Li-Ion Batteries. *Chem. Mater.* **2005**, 17, 6327-6337.
8. Larcher, D.; Sudant, G.; Leriche, J.-B.; Chabre, Y.; Tarascon, J.-M. The Electrochemical Reduction of Co<sub>3</sub>O<sub>4</sub> in a Lithium Cell. *J. Electrochem. Soc.* **2002**, 149, A234-241.

9. Doe, R. E.; Persson, K. A.; Meng, Y. S.; Ceder, G. First-Principles Investigation of the Li–Fe–F Phase Diagram and Equilibrium and Nonequilibrium Conversion Reactions of Iron Fluorides with Lithium. *Chem. Mater.* **2008**, 20, 5274-5283.
10. Boyanov, S.; Bernardi, J.; Gillot, F.; Dupont, L.; Womes, M.; Tarascon, J.-M.; Monconduit, L.; Doublet, M.-L. FeP: Another Attractive Anode for the Li-Ion Battery Enlisting a Reversible Two-Step Insertion/Conversion Process. *Chem. Mater.* **2006**, 18, 3531-3538.
11. Boyanov, S.; Womes, M.; Monconduit, L.; Zitoun, D. Mossbauer Spectroscopy and Magnetic Measurements As Complementary Techniques for the Phase Analysis of FeP Electrodes Cycling in Li-Ion Batteries. *Chem. Mater.* **2009**, 21, 3684-3692.
12. Ulldemolins, M. Study of silicon (and germanium) thin films as negative electrode for lithium-ion (micro)battery. PhD Thesis, Bordeaux University 1, Bordeaux, France, 2013.
13. Key, B; Morcrette, M.; Tarascon, J.-M.; Grey, C. P. Pair Distribution Function Analysis and Solid State NMR Studies of Silicon Electrodes for Lithium Ion Batteries: Understanding the (De)lithiation Mechanisms. *J. Am. Chem. Soc.* **2011**, 133, 503-512.

14. Sougrati, M. T.; Fullenwarth, J.; Debenedetti, A.; Fraisse, B.; Jumas, J. C.; Monconduit, L. TiSnSb a new efficient negative electrode for Li-ion batteries: mechanism investigations by *operando*-XRD and Mössbauer techniques. *J. Mater. Chem.* **2011**, 21, 10069-10076.
  
15. Marino, C.; Sougrati, M. T.; Gerke, B.; Pöttgen, R.; Huo, H.; Ménétrier, M.; Grey, C. P.; Monconduit, L. Role of Structure and Interfaces in the Performance of TiSnSb as an Electrode for Li-Ion Batteries. *Chem. Mater.* **2012**, 24, 4735-4743.
  
16. Marino, C.; Darwiche, A.; Dupré, N.; Wilhelm, H. A.; Lestriez, B.; Martinez, H.; Dedryvère, R.; Zhang, W.; Ghamouss, F.; Lemordant, D.; Monconduit, L. Study of the Electrode/Electrolyte Interface on Cycling of a Conversion Type Electrode Material in Li Batteries. *J. Phys. Chem. C* **2013**, 117, 19302-19313.
  
17. Wilhelm, H. A.; Marino, C.; Darwiche, A.; Monconduit, L.; Lestriez, B. Significant electrochemical performance improvement of TiSnSb as anode material for Li-ion batteries with composite electrode formulation and the use of VC and FEC electrolyte additives. *Electrochem. Commun.* **2012**, 24, 89-92.

18. Leriche, J.-B.; Hamelet, S.; Shu, J.; Morcrette, M.; Masquelier, C.; Ouvrard, G.; Zerrouki, M.; Soudan, P.; Belin, S.; Elkaïm, E.; Baudelet, F. An Electrochemical Cell for *Operando* Study of Lithium Batteries Using Synchrotron Radiation. *J. Electrochem. Soc.* **2010**, 157, A606-A610.
  
19. Grosse, G. *PC-Mos II; 1.0 ed.*; Technische Universität München Munich (Germany), **1993**.
  
20. Massiot, D.; Fayon, F.; Capron, M.; King, I.; Le Calvé, S.; Alonso, B.; Durand, J. O.; Bujoli, B.; Gan, Z.; Hoatson, G. Modelling one- and two-dimensional solid-state NMR spectra. *Magn. Reson. Chem.* **2002**, 40, 70-76.
  
21. Robert, F.; Lippens, P.-E.; Olivier-Fourcade, J.; Jumas, J.-C.; Gillot, F.; Morcrette, M.; Tarascon, J.-M. J. Mössbauer spectra as a “fingerprint” in tin–lithium compounds: Applications to Li-ion batteries. *Solid State Chem.* **2007**, 180, 339-348.
  
22. Dunlap, R. A.; Small, D. A.; MacNeil, D. D.; Obrovac, M. N.; Dahn, J. R. A Mössbauer effect investigation of the Li–Sn system. *J. Alloys Compd.* **1999**, 289, 135-142.

23. Conte, D. E.; Mouyane, M.; Stievano, L.; Fraisse, B.; Sougrati, M. T.; Olivier-Fourcade, J.; Willmann, P.; Jordy, C.; Cassaignon, S.; Driezen, K.; Jumas, J.-C. A combined Mössbauer spectroscopy and x-ray diffraction *operando* study of Sn-based composite anode materials for Li-ion accumulators. *J. Solid State Electrochem.* **2012**, 16, 3837-3848.
24. Meyer, B. M.; Leifer, N.; Sakamoto, S.; Greenbaum, S. G.; Grey, C. P. High Field Multinuclear NMR Investigation of the SEI Layer in Lithium Rechargeable Batteries. *Electrochem. Solid-State Lett.*, **2005**, 8, A145-148.
25. Aurbach, D. Review of selected electrode–solution interactions which determine the performance of Li and Li ion batteries. *J. Power Sources*, **2000**, 89, 206-218.
26. Bekaert, E.; Robert, F.; Lippens, P. E.; Ménétrier, M.  $^7\text{Li}$  NMR Knight Shifts in Li–Sn Compounds: MAS NMR Measurements and Correlation with DFT Calculations. *J. Phys. Chem. C* **2010**, 114, 6749-6754.
27. Chang, D.; Hua, H.; Johnston, K. E.; Ménétrier, M.; Monconduit, L.; Grey, C. P.; Van der Ven, V. Elucidating the origins of phase transformation hysteresis during electrochemical cycling of Li–Sb electrodes. *J. Mater. Chem. A* **2015**, 3, 18928-18943.

## Figure Captions

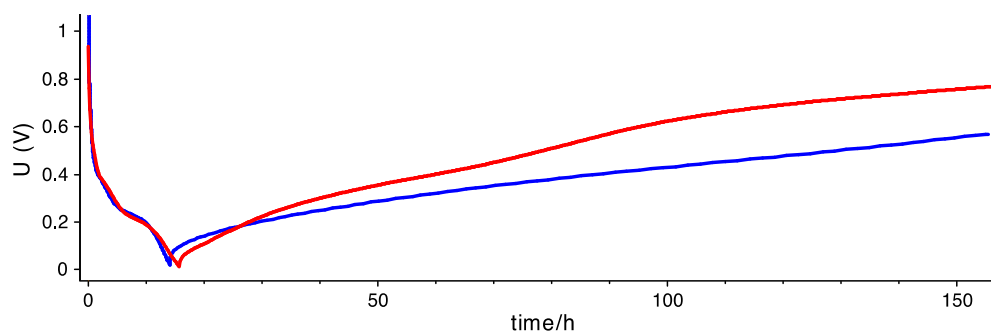


Figure 1: Potential profiles for TiSnSb obtained during *in situ*  $^{119}\text{Sn}$  Mössbauer spectroscopy experiments in the *in situ* Swagelok<sup>TM</sup> cell (blue) and  $^7\text{Li}$  NMR experiments using a two-electrode Swagelok<sup>TM</sup>-type cell with two beryllium windows (red). Samples were cycled at a rate of C/2.

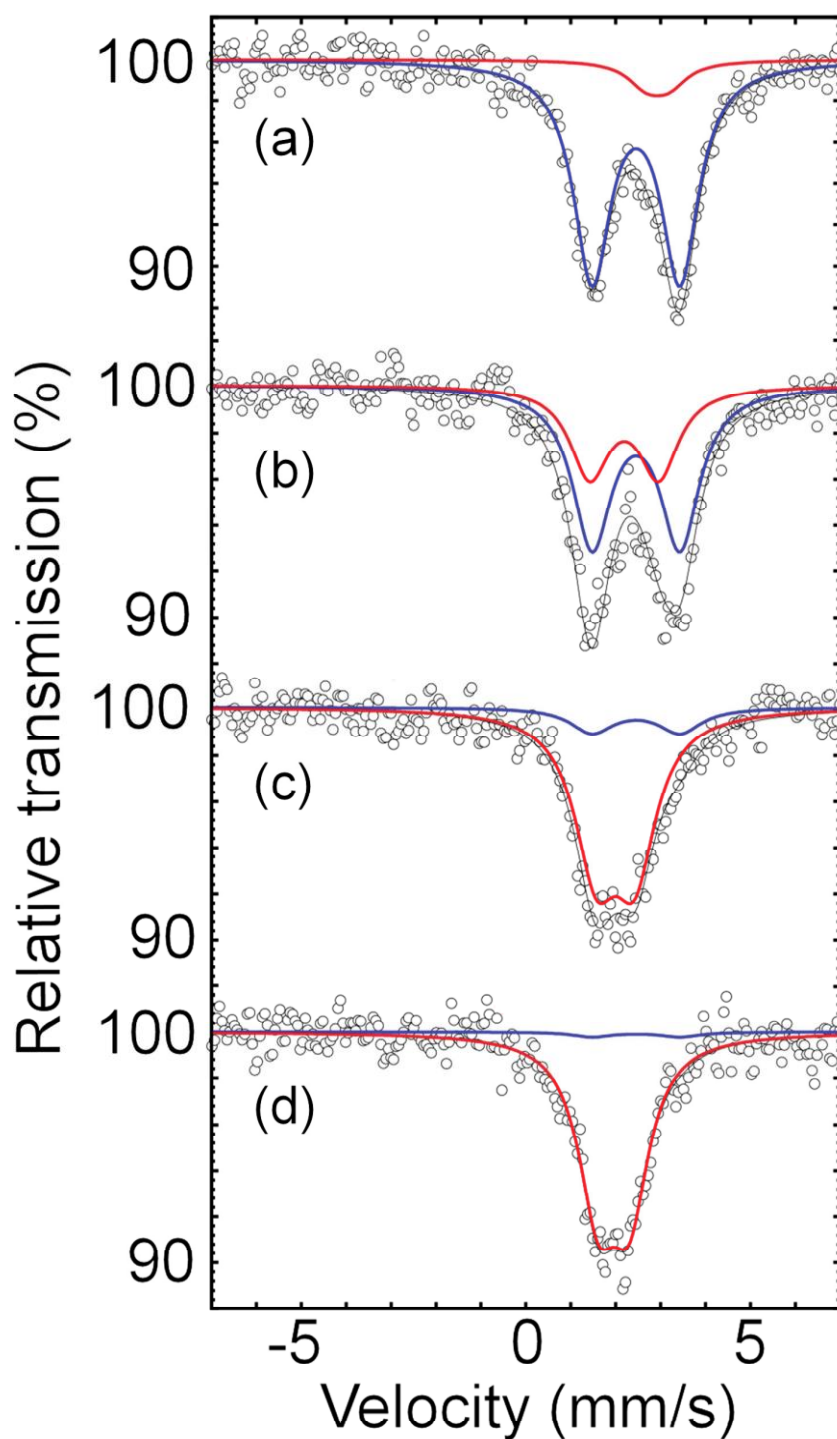


Figure 2:  $^{119}\text{Sn}$  Mössbauer spectra collected during the discharge of  $\text{TiSnSb}$  at a rate of  $C/2$ : (a) pristine material, and after (a) 5 hrs, (b) 10 hrs and (c) 14 hrs (end of discharge). Dots represent the experimental data, thick lines are the components used to fit the spectra and thin grey lines are the sum of the components. The blue component represents  $\text{TiSnSb}$ .

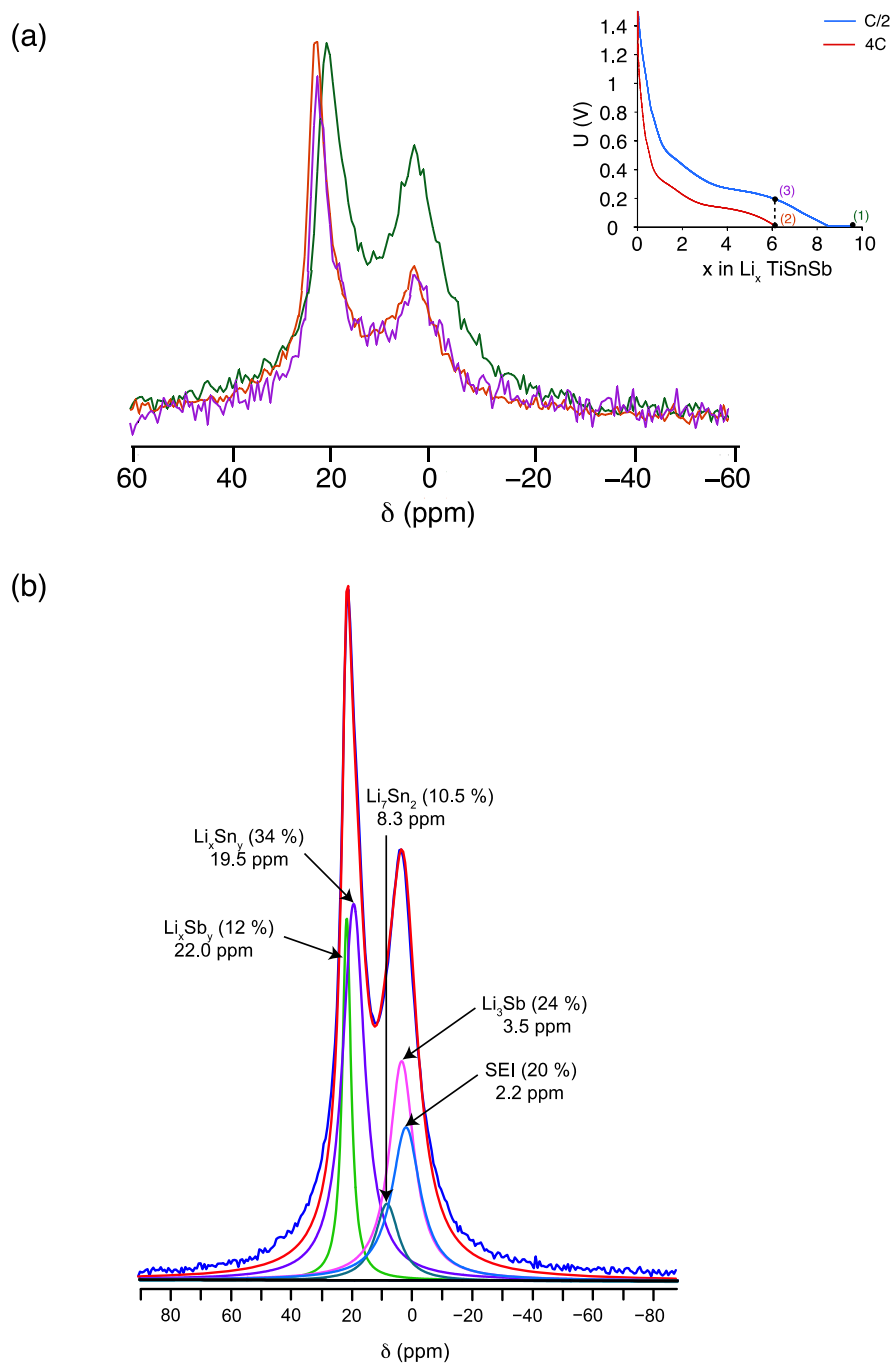


Figure 3: (a)  $^7\text{Li}$  MAS NMR spectra obtained after one discharge of  $\text{TiSnSb}$  electrodes at a rate corresponding to C/2 (green), 4C (purple) and C/2 with a specific capacity similar to that obtained for a full discharge at 4C (red). Also shown as an inset in (a) are the corresponding potential profiles. (b) Deconvolution of the  $^7\text{Li}$  NMR spectrum obtained at the end of discharge at C/2.

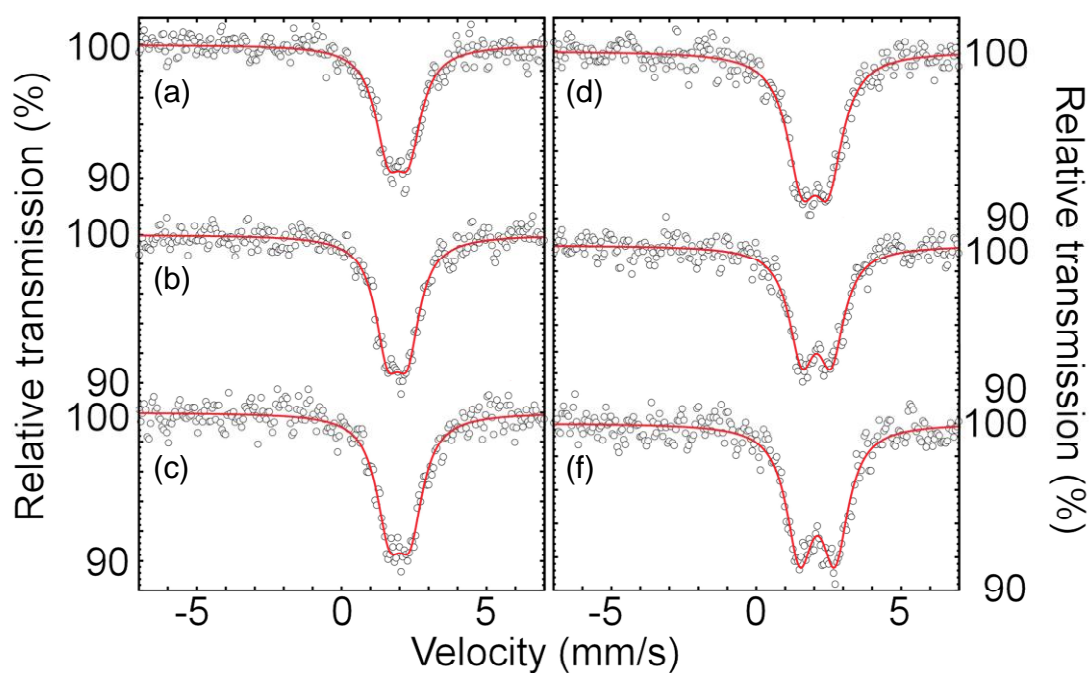


Figure 4: Selected  $^{119}\text{Sn}$  Mössbauer spectra collected during relaxation of discharged  $\text{TiSnSb}$ . Spectra obtained at (a) 14 h, (b) 30 h, (c) 50 h, (d) 70 h, (e) 100 h and (f) 150 h are shown, corresponding to potentials 0.13 V, 0.22 V, 0.29 V, 0.35 V, 0.44 V and 0.55 V, respectively. Dots represent the experimental data and the red lines are the components used to fit the spectra.

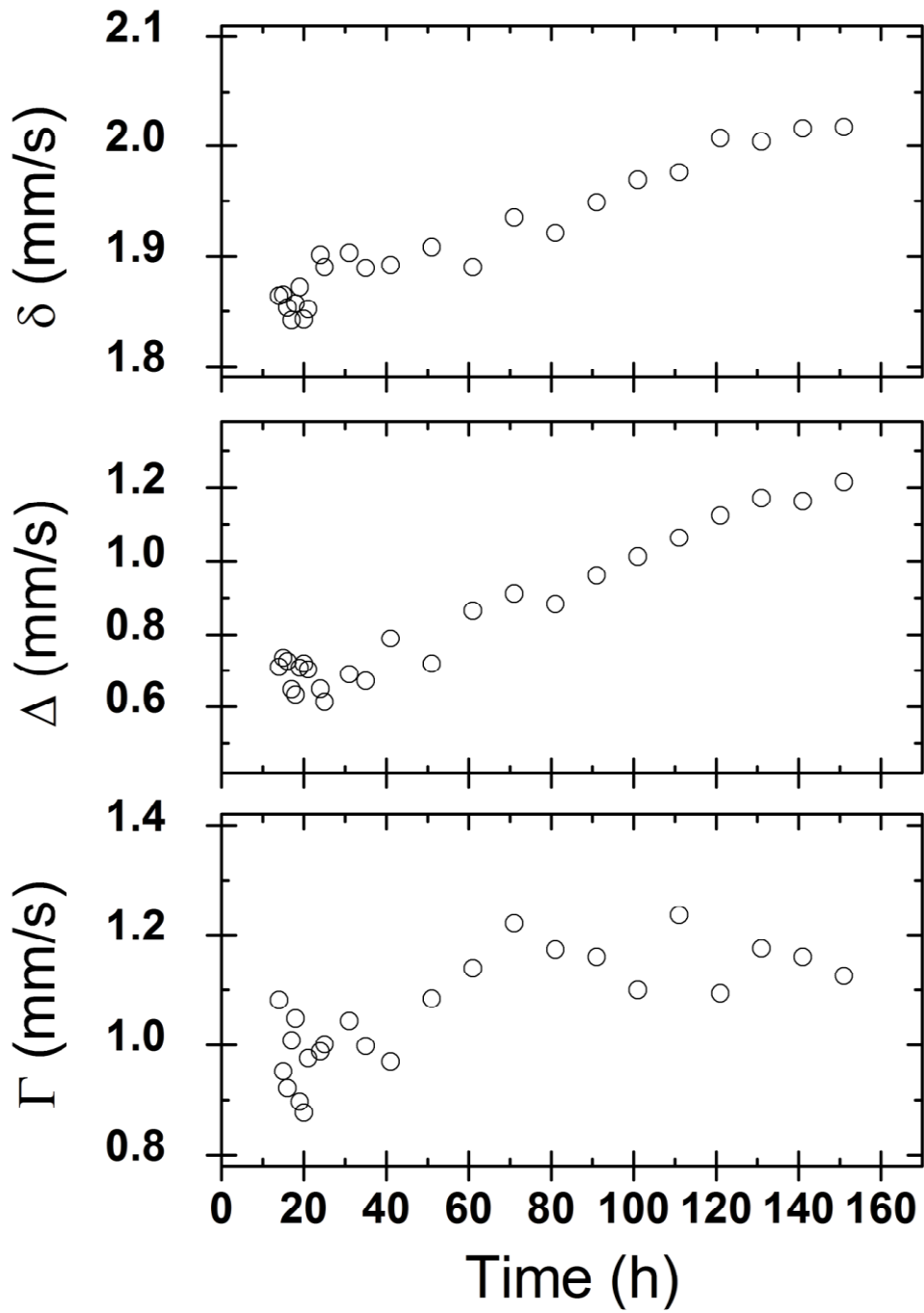


Figure 5: Evolution of the average  $^{119}\text{Sn}$  Mössbauer hyperfine parameters during the *in situ* relaxation of discharged  $\text{TiSnSb}$ : the isomer shift ( $\delta$ ), quadrupole splitting ( $\Delta$ ) and full width at half maximum ( $\Gamma$ ) parameters of the quadrupole doublet used to fit the experimental data are shown.

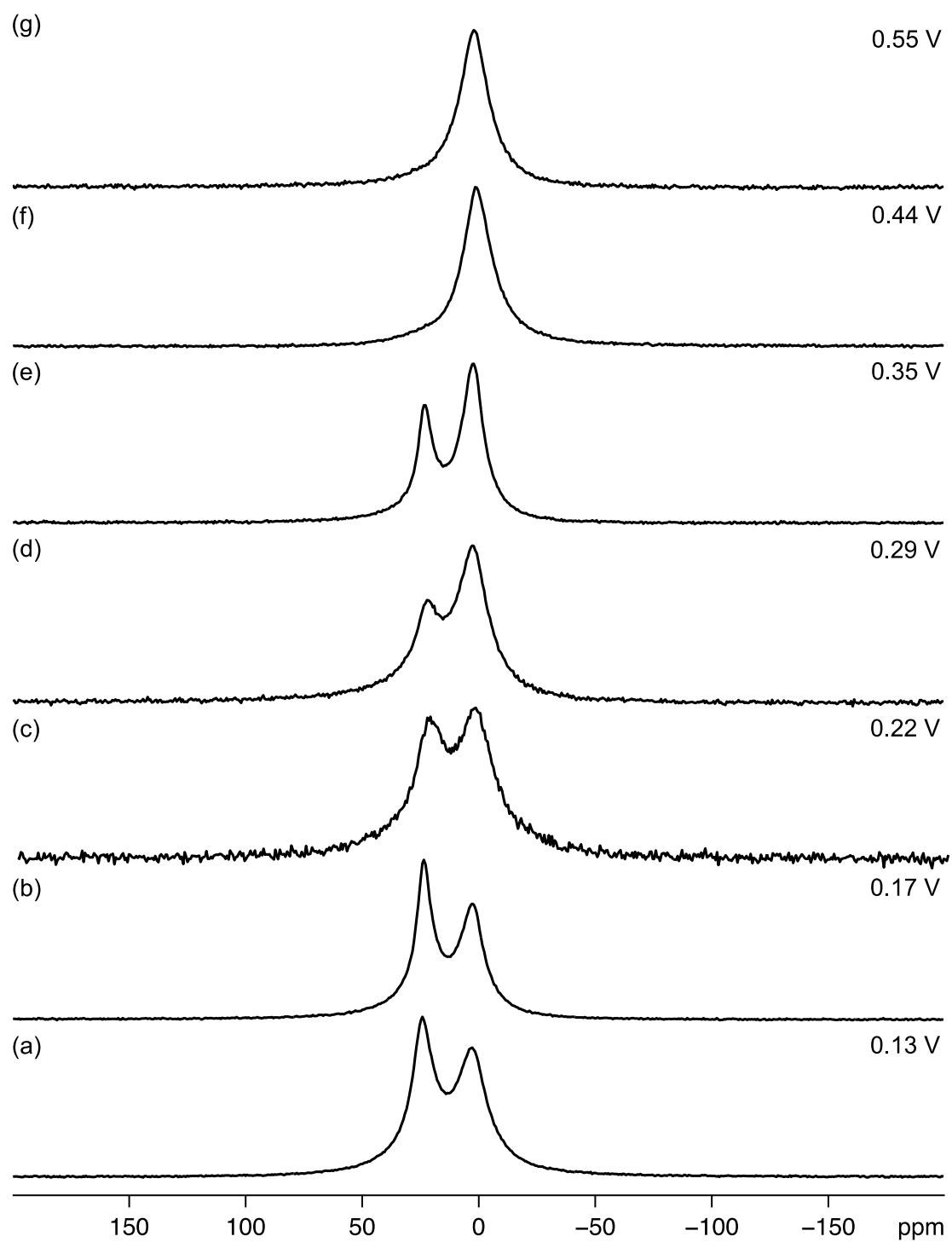


Figure 6:  $^7\text{Li}$  NMR spectra obtained after one discharge of a TiSnSb electrode at a rate corresponding to  $C/2$  and relaxation to (a) 0.13 V, (b) 0.17 V, (c) 0.22 V, (d) 0.29 V, (e) 0.35 V, (f) 0.44 V and (g) 0.55 V.

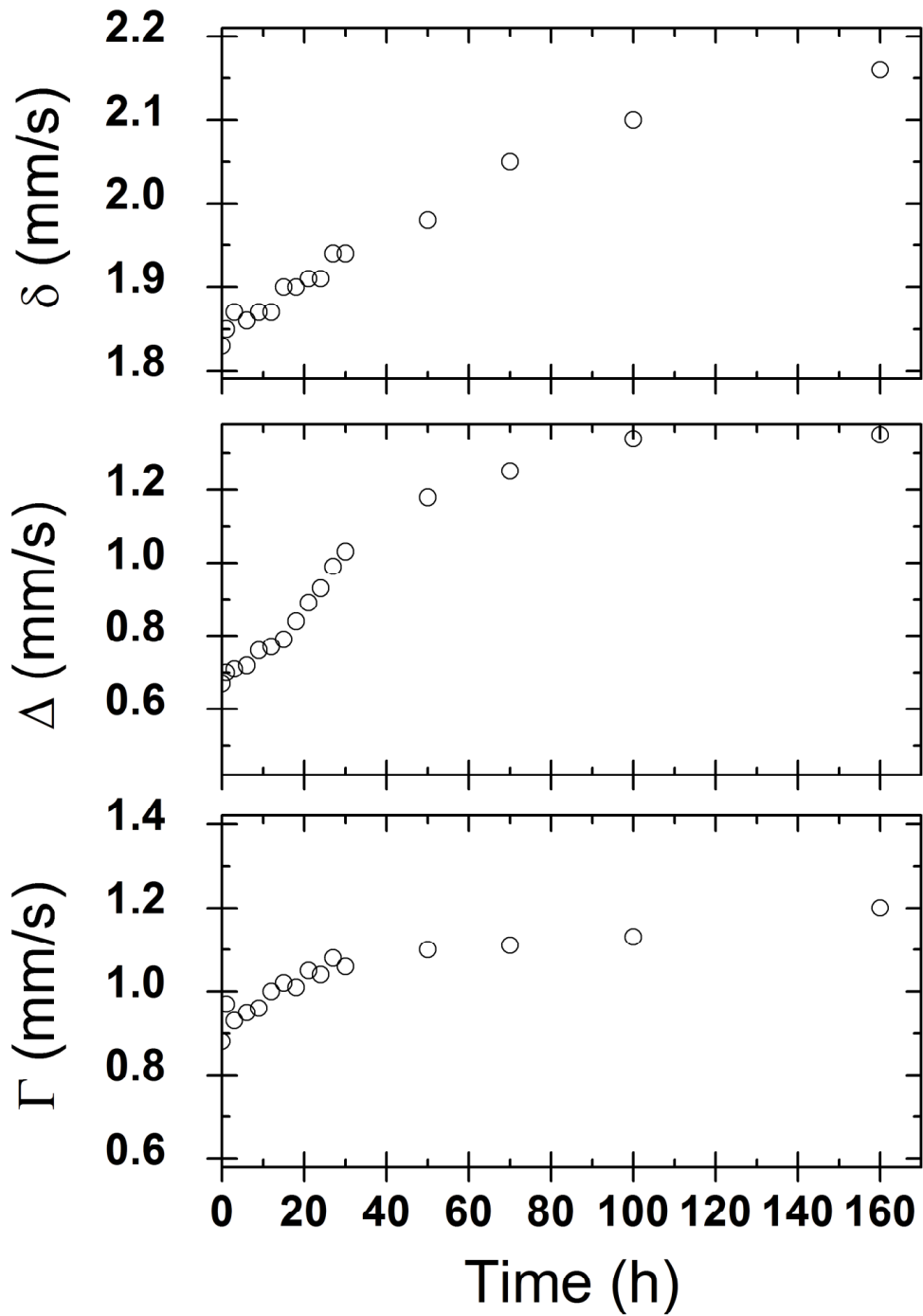


Figure 7: Evolution of the average  $^{119}\text{Sn}$  Mössbauer hyperfine parameters during the *ex situ* relaxation of discharged TiSnSb: the isomer shift ( $\delta$ ), quadrupole splitting ( $\Delta$ ) and full width at half maximum ( $\Gamma$ ) parameters of the quadrupole doublet used to fit the experimental data are shown.

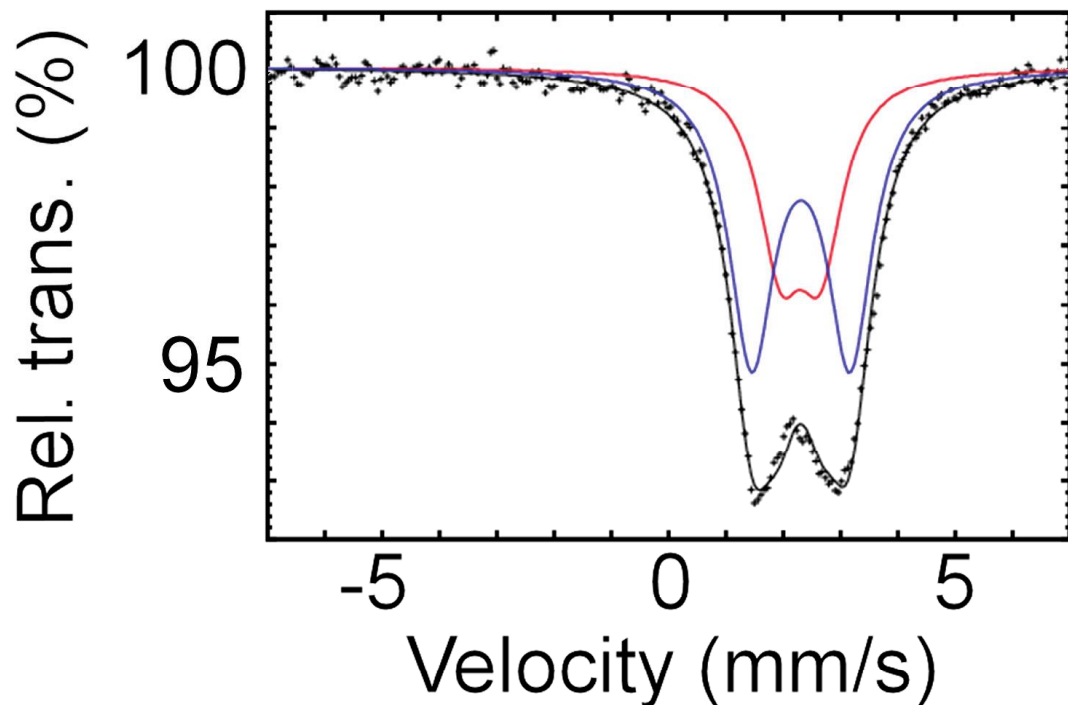


Figure 8:  $^{119}\text{Sn}$  Mössbauer spectrum collected at the end of the *ex situ* relaxation of discharged TiSnSb (160 hours), simulated using two spectral components.

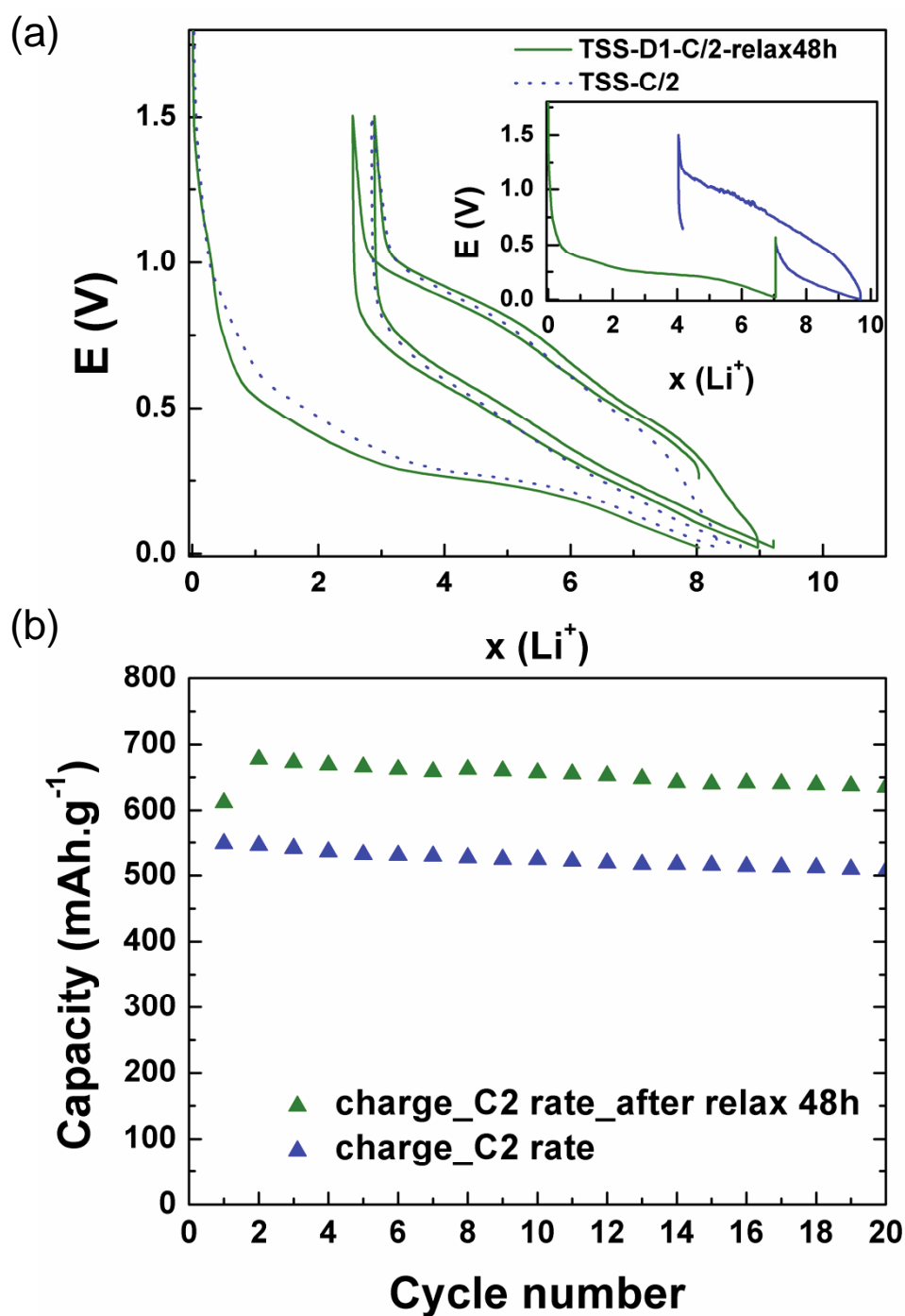


Figure 9: (a) Galvanostatic curve of TiSnSb vs. Li cycled at C/2 in classical cycling (dashed line), with a 48 h relaxation time at the end of discharge (green line) before the charge and, shown as an inset, with 150 h relaxation time at the end of discharge before a further discharge. (b) Capacity retention as a function of the number of cycles for the cycling with and without relaxation time at 0 V.

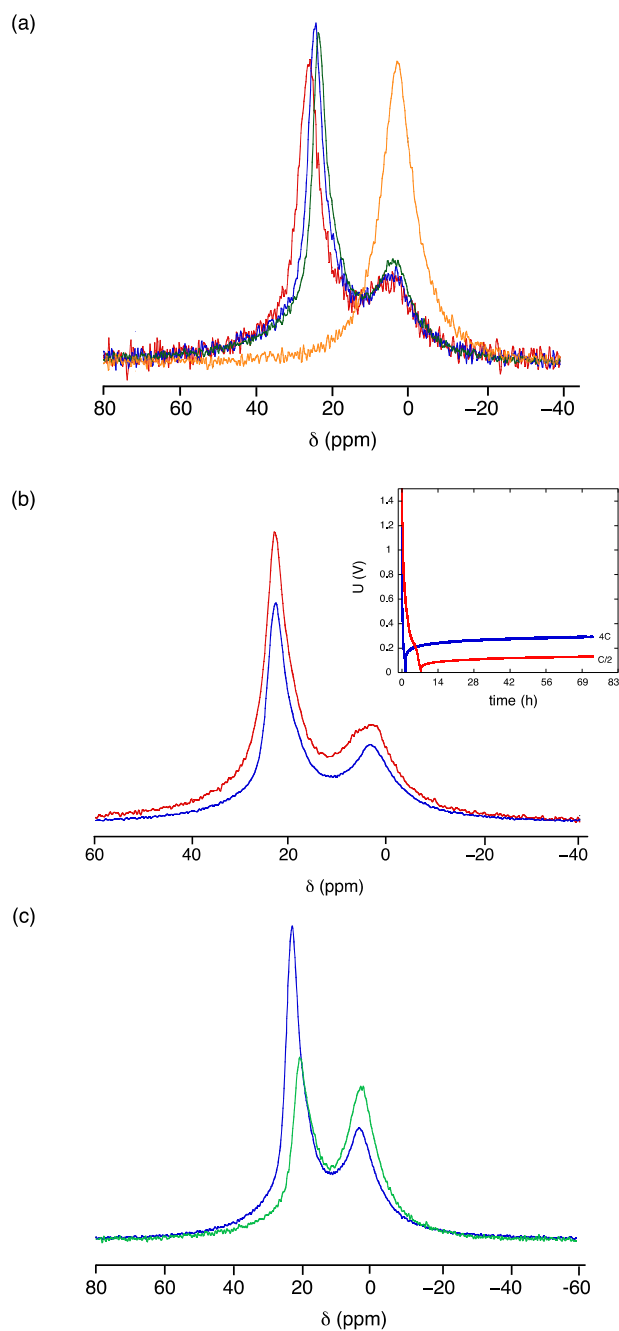
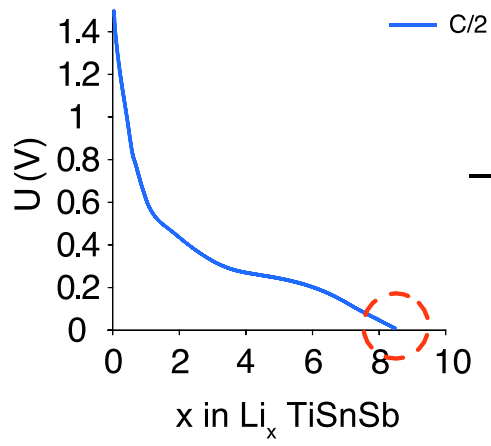


Figure 10: (a)  ${}^7\text{Li}$  NMR spectra obtained after one discharge of a TiSnSb electrode at 4C, acquired immediately after cycling (red), after 6 hours (blue), after 24 hours (green) and after 3 days (orange). (b)  ${}^7\text{Li}$  NMR spectra obtained for TiSnSb electrodes discharged at C/2 (red) and 4C (blue), followed by 72 hours of relaxation prior to disassembling the cell and (c) the sample cycled at 4C in (b) after storage in a glovebox for an additional three days (green). Also shown as an inset in (b) are the corresponding potential profiles.

## TOC Graphic

Discharged TiSnSb electrode



$^7\text{Li}$  Solid-State NMR

